Journal of Catalysis 260 (2008) 93–102

Contents lists available at ScienceDirect

Journal of Catalysis

www.elsevier.com/locate/jcat

Vanadium-promoted Pt/CeO_2 catalyst for water–gas shift reaction

Andréa M. Duarte de Farias [a], Pascal Bargiela [b], Maria da Graça C. Rocha [b], Marco A. Fraga [a,*]

[a] Laboratório de Catálise, Instituto Nacional de Tecnologia/MCT, Av. Venezuela, 82/518, Centro, 20081-312, Rio de Janeiro/RJ, Brazil
[b] Instituto de Química, Universidade Federal da Bahia, Salvador/BA, Brazil

ARTICLE INFO

Article history:
Received 26 February 2008
Revised 4 September 2008
Accepted 8 September 2008
Available online 5 October 2008

Keywords:
Water–gas shift
Fuel cell
Vanadium
Ceria
XPS
DRIFTS

ABSTRACT

Water–gas shift reaction has found new purpose and challenges due to its application in clean power generation systems based on fuel cells. It has been shown that the catalysts performance is dependent on both the metal phase and the nature of the support. In this contribution the modification of Pt/CeO_2 catalyst with vanadium was exploited. Spectroscopic techniques revealed that distinct dispersed VO_x species were generated onto the catalysts by using different vanadium loadings. The reduction of the catalysts and CO adsorption were monitored by infrared spectroscopy. It was found that the formation/decomposition of surface carbonates is affected by vanadium. Generation of multicoordinated carbonates is inhibited due to the decrease of the exposed cerium surface cations. The catalytic activity increased up to a vanadium surface density of 6 V atoms/nm^2. Improvement in water–gas shift reaction kinetics is associated with the V–O–Ce bonds.

1. Introduction

The water–gas shift reaction (WGS) is a well established industrial process. It has been particularly applied in large steady-state operations such as ammonia production plants. More recently, it has found new purpose and challenges due to its application in clean power generation systems based on proton exchange membrane (PEM) fuel cells. Nevertheless, in order to fit the demanding requirements imposed by such technology, the development of new advanced catalysts is mandatory. A compact fuel processor system may only be available by using more active WGS catalysts, as large volumes of shift reactors are currently necessary, being responsible for about 50% of the volume of the whole fuel processor [1]. Moreover, taking into account the operational cycles of a fuel cell as well as the actual reformer outlet composition, the catalyst deactivation must also be carefully considered. So far, only few papers have dealt with the deactivation process arising from these operating conditions [2,3]. These contributions indicate that depending on the formulation of the catalyst the deactivation is driven by different phenomena. Undoubtedly, this is a complex theme that still demands further investigations; articles deeply dedicated to it are just beginning to appear in the literature.

The possibility of methane formation from hydrogen and CO in the reformate [4,5], which would decrease the H_2/CO ratio, is another relevant issue that should also be evaluated when designing new catalysts for hydrogen purification by WGS.

Since it is reversible and exothermic ($\Delta H_{25\,^\circ C} = -41.2$ kJ/mol), the reaction is favored at low temperatures and with excess of steam. Industrially, larger CO conversions are accomplished by carrying out the reaction over two different materials depending on the temperature adopted; high temperature shift—HTS (350–450 °C) on FeCr-based catalysts and low temperature shift—LTS (180–250 °C) on CuZn-based systems. Supported noble metal catalysts have also been considered for the WGS reaction as they combine high activity and stability. Even though they have been extensively studied as LTS catalysts [6–11], some results have also been reported at high temperature conditions [12]. Therefore, they are quite interesting candidates to perform the reaction in a single step at an intermediate temperature, a medium temperature shift catalyst. Such accomplishment would meet the demand for power generation through hydrogen-fueled PEM cells in small fuel processor systems.

Amongst the noble metals, platinum and gold are by far the most studied ones. Platinum catalysts are generally more active than ruthenium, rhodium and palladium [13] but when contrasted with gold, its catalytic performance seems to be controversial. Some authors claim that gold-based systems are excellent LTS catalysts when compared to the platinum systems [6,11,14]. They have also suggested that such activity is due to active non-metallic gold species. Conversely, some other results have showed that platinum/ceria is far more effective than gold and that metallic platinum species play an important role in the catalysis [9].

Not only has the catalysts performance been shown to depend on the metal phase but also on the nature of the support used. Mining the literature one can easily see that a wide variety of oxides has been tested in WGS reaction. Ceria, alumina, zirconia,

* Corresponding author. Fax: +55 21 21231166.
E-mail address: marcofra@int.gov.br (M.A. Fraga).

0021-9517/$ – see front matter
doi:10.1016/j.jcat.2008.09.004

titania, thoria and magnesia may be listed among them [15–19]. Yet, it has been recognized that higher activities are achieved by reducible oxides much likely due to their redox properties and their crucial role as a source of oxygen. Despite their superior performance, distinct reducible oxides have shown to be differently affected by their structural and morphological characteristics. As for ceria, which is undoubtedly the most investigated support; its behavior seems not to be influenced by crystallite size in a strong contrast to what has been found for titania [13].

Other studies have sought to improve WGS reaction by incorporating different compounds into the traditional bare oxides and some improvement was reached in certain cases. In a previous work, we showed that the association of a reducible support (CeO_2) with centers capable of promoting the decomposition of the intermediate formate species (MgO) indeed led to a better catalytic performance [19]. Similarly, some authors have doped ceria with lanthanides cations in order to obtain mixed oxides with improved reducibility [20,21]. The present scenario on WGS studies indeed reveals that improved redox properties seem to positively influence both redox and formate mechanisms.

Only few papers can be found in the scientific literature regarding the use of vanadium in WGS catalytic systems either as a catalyst or as a promoter [22,23]. On the other hand, vanadium oxide has largely been used in oxidation reactions and it is known to present high oxygen mobility when partially reduced. This characteristic is also a consequence of the capacity of structural defect generation [24], which makes vanadium a worth investigating compound for the WGS reaction.

Ballarini et al. [22] studied bulk and supported V_2O_5 for the oxidation of propane. The choice of the correct propane/O_2 ratio showed to favor the occurrence of the WGS reaction during this process. The reducing atmosphere inside the reactor caused the formation of V_2O_3 which was considered to be the active phase in WGS at temperatures above 450 °C. Bulk V_2O_5 was also investigated in the WGS using the reformate from both methanol and methane as reactants [4]. So far, that is the sole contribution that mentions the association of a metal with a V-based support for the WGS reaction. The authors studied the behavior of Ru catalysts and observed that, among other supports, reduced V_2O_5 presented the best performance. However, it should be outlined that a critical investigation of the correlation between the active vanadium structures and the WGS mechanisms is still missing. We have also reported a brief evaluation of a vanadium-modified Pt/CeO_2 catalyst elsewhere [23] revealing that this system was more active than the widely studied Pt/CeO_2. It was then suggested to be related to the redox properties of a crystalline V_2O_5 phase identified by X-ray diffraction and Raman spectroscopy. Such results associated with the rather complex chemistry of vanadium compounds, especially its capacity to form different mono-, bi- and tridimensional structures, motivated a more detailed investigation on this system.

Therefore, the present contribution aims at describing the vanadium structures generated on a Pt/CeO_2 catalyst and their possible role in modifying or acting as the reactive sites in the WGS reaction. Thus, a series of spectroscopic techniques was used in order to identify the possible species involved. This information will be handled to evaluate the use of vanadium as a promoter for medium temperature WGS catalysts applying as reactants an ethanol reformate.

2. Experimental

2.1. Catalysts preparation

A high surface area cerium oxide support was prepared by a method described in detail elsewhere [25]. Briefly, it was synthesized by precipitation from an aqueous solution of cerium(IV) ammonium nitrate (Aldrich) with NH_4OH. After extensive washing until constant pH, the solid was calcined at 500 °C for 1 h.

Four modified supports were prepared by wet impregnation with an aqueous solution of NH_4VO_3 (Merck) and oxalic acid (Merck), with a 2:1 molar ratio, in which the concentration was calculated to result in different vanadium loadings. The solution containing all precursors was added to ceria and the resulting suspension was kept under agitation in a rotary evaporator for 4 h at room temperature. Afterwards, water was slowly removed at 65 °C under vacuum. The solids were then dried at 120 °C and calcined at 500 °C for 2 h under air flow at 30 $cm^3\,min^{-1}$.

Pt/CeO_2 and the modified catalysts were prepared by incipient wetness impregnation with an aqueous solution of H_2PtCl_6 so as to obtain a platinum content of 1 wt%. The powders obtained were first dried overnight at 120 °C and then submitted to a final calcination step in air stream (30 $cm^3\,min^{-1}$) at 500 °C for 4 h.

Both supports and catalysts were labeled according to their chemical composition.

2.2. Standard characterization

X-ray diffraction (XRD) patterns of the prepared supports were collected in a Rigaku Miniflex powder diffractometer with Cu$K\alpha$ radiation (1.5406 Å), operating at 30 kV and 40 mA. Analyses were carried out with a 0.05°/step and 2 s/step over a 2θ range of 20°–80°. Scherrer equation was used to estimate the crystallite mean diameter based on the (111) CeO_2 plane.

Surface area measurements were obtained from nitrogen adsorption at −196 °C in a Micromeritics ASAP 2010 equipment. Prior to the analyses, the samples were degassed at 150 °C. The specific surface areas were determined by BET method.

The catalysts actual chemical composition was determined by X-ray fluorescence analyses, which were carried out in a Bruker spectrometer, model S-4 Explorer.

Infrared spectra of the powders were collected in a Nicolet Magna 560 spectrometer. The samples were pressed with KBr (3 wt%) and the measurements were taken from 4000 to 400 cm^{-1} with a resolution of 4 cm^{-1}.

2.3. Diffuse reflectance UV–vis spectroscopy (DRS)

UV–vis spectra were collected in a Varian Cary 5 spectrophotometer (Harrick Scientific) with a diffuse reflectance accessory of Praying Mantis geometry. The samples were set in holds with 2 mm thickness. The respective CeO_2 support was used as reference compound. The spectra were recorded in the range between 190 and 800 nm with a scanning speed of 1800 nm/min.

2.4. X-ray photoelectronic spectroscopy (XPS)

Measurements were taken in a VG ESCALAB MKII instrument with a hemispherical electron analyzer. Non-monochromatic Mg$K\alpha$ radiation ($h\nu = 1253.6$ eV) was used as the X-ray source. The pass energy for the high resolution spectra was 50 eV. The samples were analyzed in the UHV (10^{-8} mbar). The spectra were referenced to the C1*s* emission at 284.8 eV.

2.5. Diffuse reflectance infrared spectroscopy (DRIFTS)

DRIFTS analyses were used for monitoring the catalysts reduction and CO adsorption. The experiments were carried out in a Nicolet Magna 560 spectrometer, equipped with a high temperature chamber fitted with ZnSe windows (SpectraTech), which was used as shift reactor for *in situ* measurements. Spectra were taken at resolution of 4 cm^{-1} and 256 scans to improve the signal to

Table 1
Chemical composition, surface area and CeO_2 mean crystallite size of all samples

Sample	Pt (wt%)[a]	V_2O_5 (wt%)	S_{BET} ($m^2\,g^{-1}$)	d_{CeO_2} (nm)
V_2O_5	–	–	7	–
CeO_2	1.18	–	93	8.17
$1VCeO_2$	1.13	1.40	68	8.10
$6VCeO_2$	1.15	5.92	65	8.13
$12VCeO_2$	1.09	14.38	50	8.36
$18VCeO_2$	1.08	19.14	35	8.65

[a] Pt loading present on the parent catalysts.

noise ratio. The reduction step was followed by admitting hydrogen into the cell and collecting spectra at different temperatures after 30 min at each temperature. CO adsorption was monitored using a 3 vol% CO/N_2 mixture and the same protocol was used to collect the spectra. The reduced sample was used as background.

2.6. Catalytic evaluation

Prior to reaction, the WGS catalysts were submitted to *in situ* reduction step at 350 °C for 1 h under pure hydrogen flow (30 $cm^3\,min^{-1}$).

The reaction was carried out at different temperatures within 200–350 °C and was conducted with different residence times depending on the type of experiment. Reaction rates were determined under differential conditions and the evolution of conversion as a function of reaction temperature was performed with $W/Q = 0.8\ g\,s/cm^3$. To simulate the conditions found at the outlet of a fuel ethanol reformer, a gas reactant mixture with composition 6.0% CO, 16.0% H_2, 1.6% CO_2, 0.4% CH_4, 60.0% H_2O and N_2 (balance) was used. It must be emphasized that it corresponds to the wet reformate composition, which was provided by adding an excess amount of steam into the original ethanol reformate stream reported elsewhere [26,29].

In order to avoid temperature gradients in the reactor, silicon carbide was added for dilution ($w_{cat}/w_{dil} = 1/5$) to form a small catalyst bed (<10 mm in height). The temperature of the catalyst bed was measured through a thermocouple inserted in a small cavity on the reactor outside wall.

The reaction was performed at atmospheric pressure in a conventional system with fixed bed U-shaped reactor with a 13 mm inner diameter attached to a TCD gas chromatograph (Agilent 6890N) equipped with a packed column Supelco (HayeSep Q) associated with a molecular sieve.

3. Results and discussion

3.1. Materials characterization

Table 1 presents the chemical analysis for all samples, showing that the actual platinum and vanadium content in the prepared catalysts are close to the nominal values.

XRD patterns of the supports are shown in Fig. 1. Almost all materials show only the reflections corresponding to the fluorite type structure of CeO_2; the basal reflections at $2\theta = 28.6°$; 33.1°; 47.5° and 56.5° are respectively associated with the planes (111), (200), (220) and (311). However, a closer analysis of the high vanadium content samples allowed identifying some small reflections related to vanadium-crystalline oxide phases. Tiny peaks at $2\theta = 26°$ may be observed on both $12VCeO_2$ and $18VCeO_2$ samples and can be attributed to the presence of a V_2O_5 phase (Fig. 1). As for the powder with the highest vanadium loading, sharper extra reflections at $2\theta = 24°$ and 32.5° can also be noted and are ascribed to the formation of a $CeVO_4$ phase. The appearance of such crystalline phase on ceria-supported vanadium has been extensively reported by other authors [28–31].

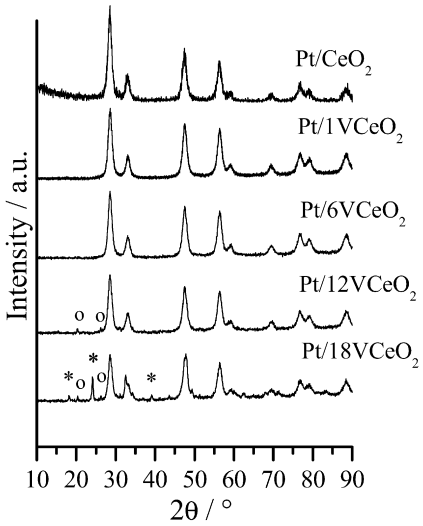

Fig. 1. XRD patterns of all prepared samples. (○) V_2O_5, (∗) $CeVO_4$.

BET surface areas are also summarized in Table 1. It can be observed that the surface area gradually decreases as the vanadium content increases. Indeed, a clear correlation can be found and is depicted in Fig. 2a. This behavior is likely bounded to the solid state reaction between ceria and vanadium, especially at high loadings, responsible for the formation of the crystalline phases revealed by XRD. The development of V^{5+}–O–Ce^{3+} sites as precursors to $CeVO_4$ upon ceria impregnation was already mentioned by Martínez-Huerta et al. [30]. The creation of such bonds was suggested to be a consequence of the ability of surface vanadia to remove the most easily reducible surface oxygen of ceria.

Accordingly, this textural change is also well represented by the enlargement of ceria crystallite size upon vanadium impregnation. Fig. 2b presents the dependence found between surface area and the mean diameter of ceria crystallites as estimated by the peak broadening in the XRD patterns according to the Scherrer equation.

The structure of the supports was also evaluated by infrared spectroscopy in the region within 600–1400 cm^{-1}, which corresponds to the V–O vibrations. Fig. 3 shows the spectra of all samples along with those corresponding to $CeVO_4$ and V_2O_5 reference materials. Vanadium oxide exhibits two main absorptions at 1023 and 823 cm^{-1} corresponding to V=O stretching and V=O and V–O–V coupled vibrations, respectively [32,33]. $CeVO_4$ presents an intense absorption at 800 cm^{-1} with a shoulder at around 737 cm^{-1} related to VO_4 units from the orthovanadate structure. As for the synthesized supports, it is possible to observe that the absorption pattern gradually changes as vanadium content increases. Only one large band is observed at 980 cm^{-1} when the vanadium concentration reaches approximately 3 wt% ($6VCeO_2$, Fig. 3). This absorption is related to V=O stretching vibration and the shift to lower wavenumbers reveals the occurrence of a highly dispersed vanadium phase. As a matter of fact, this characteristic has been described by different research groups [32,34] studying low content V_2O_5 supported on titania and titania-based mixed oxides and is generally ascribed to V=O bonds of monolayered V^{5+} species. The spectrum of $12VCeO_2$ sample, on the other hand, is featured by two broad bands at 820 and 980 cm^{-1}, which are consistent with crystalline and highly dispersed V_2O_5 configurations, respectively, suggesting the co-existence of both phases. Likewise, the $18VCeO_2$ spectrum shows strong absorptions which may be attributed to the presence of crystalline V_2O_5. Nevertheless, it must be noticed that the broad band roughly centered at 822 cm^{-1} possesses a shoulder at lower wavenumber, which may come from the $CeVO_4$ structure in a pretty good agreement with the previous XRD results.

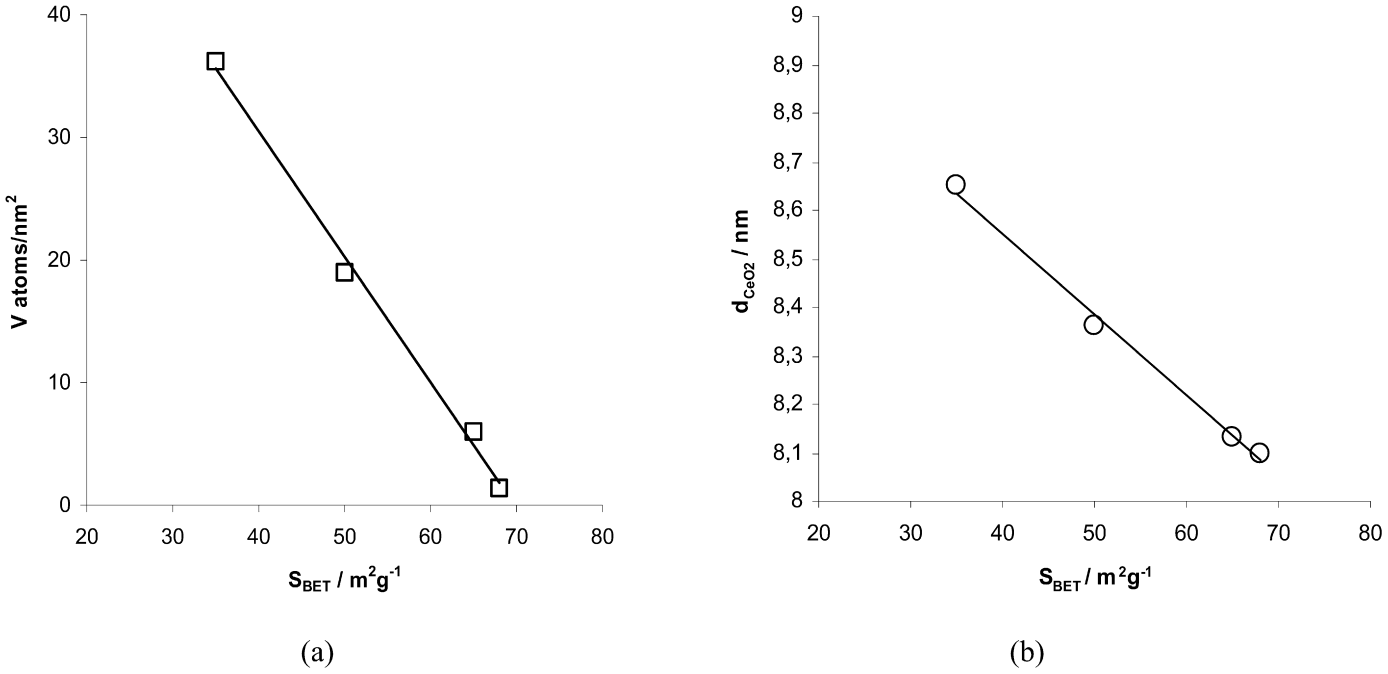

Fig. 2. Correlation between (a) vanadium density and surface area; (b) ceria crystallite size and surface area.

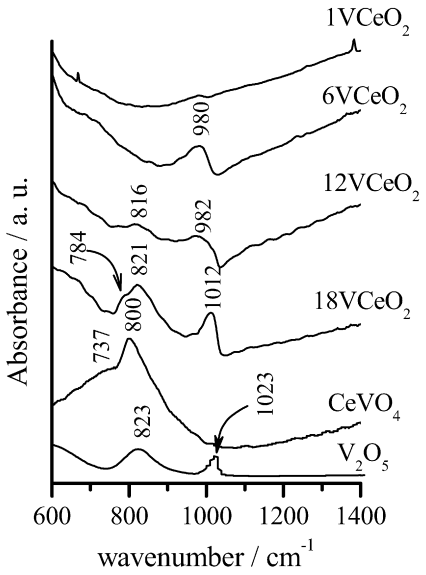

Fig. 3. Infrared spectra of prepared samples and reference materials.

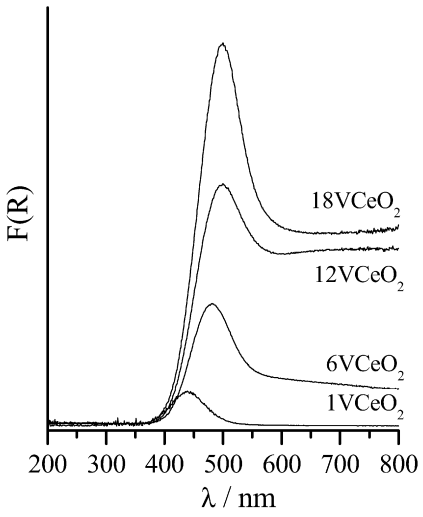

Fig. 4. DRS spectra of vanadium-modified supports.

UV diffuse reflectance spectra are presented in Fig. 4. The spectra reveal basically one absorption band. The sharp rise in absorption corresponds to the charge transfer of V^{5+} in the decavanadate structure (octahedron). It is worth noting, however, that the UV absorption shifts towards lower wavelength as vanadium loading decreases, moving from 500 to ~437 nm when concentration goes from 19 to 1 wt%. It indicates that vanadium species are more highly dispersed at low vanadium amounts, probably as monovanadate species [33,35].

It is well known that the dispersion of vanadium species onto an oxide surface is strongly dependent of the preparation variables, especially the temperature, and the chemical interaction between the support and the supported species [35,36]. Hence it is important to analyze the effects brought about by vanadium taking into account the density of VO_x species. Assuming that the formation of a vanadium monolayer on a support consists of either isolated or polymeric species, theoretical surface densities of 2.5 and 7.5 V atoms/nm^2 may be calculated for monovanadates and polyvanadates, respectively [33]. The experimental values determined for the samples in this work are collected in Table 2. It can be seen that for the samples with low vanadium content the surface density (<7.5 VO_x/nm^2) is not enough to provide a monolayer and thus only the formation of a submonolayer of nanostructured monovanadates ($1VCeO_2$) or polyvanadates ($6VCeO_2$) could be considered. As for vanadium loading from 8 wt% the density increases dramatically, above the estimated theoretical values. It should be observed that such an increase is effective no matter it is calculated based on the surface area of the starting CeO_2 support or those determined for the final modified supports. Such high densities allow the organization of the VO_x units and thus the formation of tridimensional crystalline structures such as V_2O_5 as revealed by XRD and FTIR. This indicates that it is possible to control the formation of the vanadate species through the amount of vanadium in the catalyst formulation.

Table 2
Vanadium surface densities

Sample	V (wt%)	V density[a] (V atom/nm^2)	V density[b] (V atom/nm^2)
1VCeO$_2$	0.78	1.4	0.9
6VCeO$_2$	3.32	6.0	4.0
12VCeO$_2$	8.05	19.0	9.7
18VCeO$_2$	10.72	36.2	8.65

[a] Calculated based on the BET area of the final modified support.
[b] Calculated based on the BET area of the starting CeO$_2$.

The surface of all studied samples was qualitatively and quantitatively investigated by XPS. However, a XPS analysis over vanadium compounds is not a simple task, especially when associated with cerium oxides. It must be carefully carried out due to the complex parameters concerning the nature of vanadium, mostly in oxidized form, and the variety of peaks in the Ce3*d* region as a consequence of a number of shakedowns.

As can be seen in Fig. 5a, the O1*s* and V2*p* signals are registered within the same binding energy (BE) region, especially for V2$p_{1/2}$, which makes it pretty difficult to evaluate its contribution. Moreover, the O1*s* + V2*p* region of the spectra contains another specific feature related to satellite peaks due to the hybridization between V3*d* and O2*p* levels. These satellites may be found simultaneously or not, located at different binding energies [37]. By mining the related literature it can be seen that there is a wide range of values for binding energies reported for the different oxidation states of vanadium. V^{5+} ranges between 517.5 and 518.2 eV; V^{4+} is usually located at the interval 516.5–517.1 eV and V^{3+} varies between 515.2 and 515.9 eV [38,39]. Analyzing the O1*s* + V2*p* region of our samples spectra (Fig. 5a), it is possible to recognize the growing of V^{5+} species, whose V2$p_{3/2}$ core level binding energy is between 517.7 and 517.0 eV, with the increase of vanadium content.

The identification of such oxidation state is also confirmed by calculating the binding energy difference (Δ) between the O1*s* and V2$p_{3/2}$ levels, as suggested by Silversmit et al. [38]; these values are collected in Table 3.

The deconvolution of vanadium peak (not shown) revealed that the distribution of its oxidation states becomes wider as the vanadium loading increases, making the spectra gradually more complex. The presence of at least two different V species can be claimed: V^{5+} and another lower state of oxidation, which can be identified as V^0 or V^{2+} and probably also as V^{3+}, while the V loading increases (Table 3). Contrarily, for loadings below 12 wt% the presence of a narrower distribution of oxidation states, mainly V^{5+}, agrees with the formation of dispersed VO_x species whether isolated or polymeric units. The spectra showed that, indeed, only V^{5+} is observed for Pt/1VCeO$_2$.

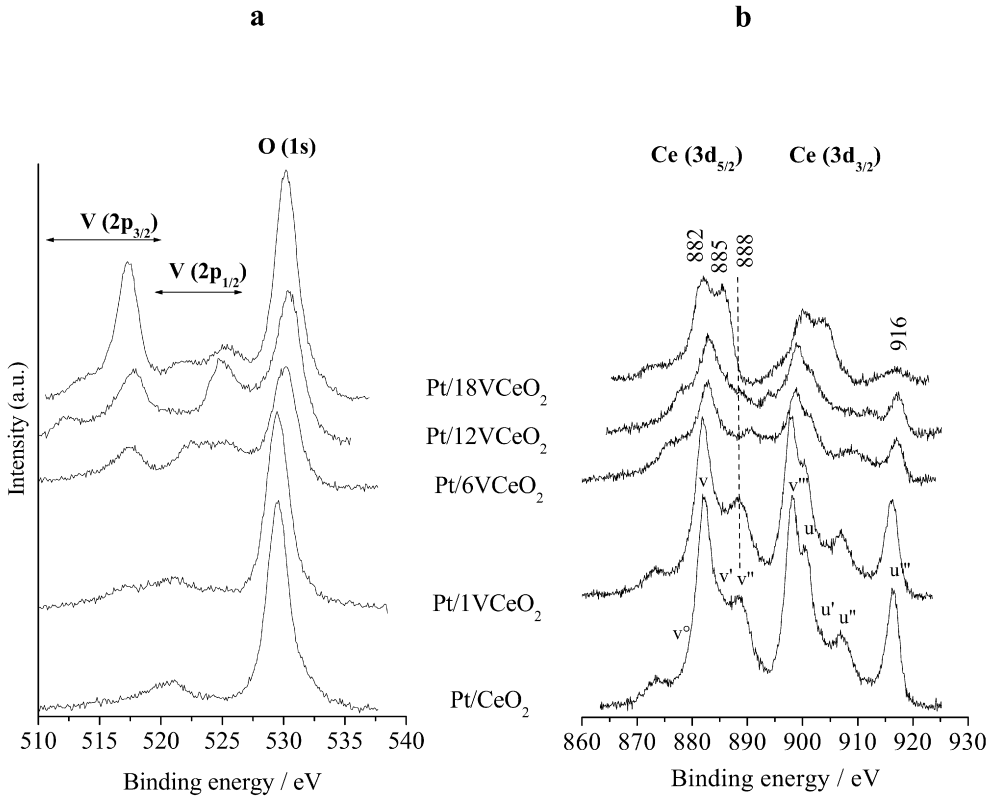

Fig. 5. XPS spectra showing the O1s + V2p (a) and the Ce3d (b) regions of the catalysts compared to Pt/CeO$_2$.

Table 3
Binding energies of V2$p_{3/2}$ level and their difference (Δ) in relation to the O1*s* level

Catalysts	V^{5+}		V^{3+}		V^{2+}		V^0	
	BE (eV)	Δ (12.8 ± 0.2)	BE (eV)	Δ (14.7 ± 0.2)	BE (eV)	Δ (16.3 ± 0.2)	BE (eV)	Δ (17.7 ± 0.2)
Pt/1VCeO$_2$	517.0	12.5	–	–	–	–	–	–
Pt/6VCeO$_2$	517.3	12.7	–	–	513.9	16.1	–	–
Pt/12VCeO$_2$	517.7	12.6	515.0	15.3	–	–	512.4	17.9
Pt/18VCeO$_2$	517.4	12.7	515.6	14.5	513.5	16.6	–	–

Δ values in parentheses were included for comparison with Ref. [38].

Table 4
Superficial atomic ratios and V2*p*, O1*s* and Ce3*d* binding energies by XPS

Samples	BE (eV)			Atomic ratios		
	$Vp_{3/2}$	O1s	Ce3d	Ce^{4+}/Ce^{3+}	Pt/(V + Ce)[a]	V/Ce[a]
Pt/CeO_2	–	529.2	882.0	9.7	0.026	–
$Pt/1VCeO_2$	517.0	529.5	881.8	11.0	0.025	0.2
$Pt/6VCeO_2$	517.3	530.0	882.0	6.3	0.023	1.6
$Pt/12VCeO_2$	517.7	530.3	882.4	7.1	0.016	2.5
$Pt/18VCeO_2$	517.4	530.1	881.7	4.2	0.011	7.8

[a] Ce^{4+} % calculated on the basis of u''' peak.

Considering the preparation method adopted in the present work, the possibility of metallic vanadium occurrence is remote. Therefore it is important to take into account the vacuum conditions underwent by the samples during the XPS experiments. A study has already revealed [39] that vanadium decreases its oxidation state under the ultra high vacuum environment inside the XPS chamber. This argument gives further support to the calculation of the Δ value as mentioned above and may indicate that the presence of V^0 does not correspond to real surface stoichiometry. Indeed it has been found that in V_2O_5 films supported on CeO_2 only submonolayer samples could totally retain V^{5+}, while for higher loading materials a small part of the vanadium content is in V^{3+} form [39].

Ce3*d* region is displayed in Fig. 5b. Some important features can be mentioned, but for a complete analysis of this region the reader is referred to the literature [40,41]. Briefly, the spectra present two principal energy spin-orbit states: $Ce3d_{5/2}$, represented by peaks labeled v, and $Ce3d_{3/2}$, labeled u. The doublet u'–v', positioned at around 904.0 and 885.0 eV, respectively, appears as a consequence of Ce^{3+} ions photoemission [42,43] and therefore these peaks can be taken as representative for the occurrence of that oxidation state. The peak at around 880.0 eV ($v°$) is a shakedown that occurs through the transference of one electron from an O2*p* orbital to a Ce4*f* during the photoemission of Ce^{3+} [42]. A satellite peak, named u''', appears at around 916.5 eV due to transitions in Ce^{4+} $4f^0$ state and composes a doublet with v''' peak (∼898 eV). It has been claimed that the u''' peak area may be used to estimate the Ce^{4+} percentage [44].

Analyzing Fig. 5b, it is seen that the deposition of only 1 wt% V_2O_5 did not seem to provoke deep changes in the spectrum when compared to the Pt/CeO_2, indicating the massive presence of Ce^{4+} species. The following spectra, on the other hand, reveals that Ce^{4+} relative population decreases and Ce^{3+} increases as vanadium content reaches higher amounts. In addition, the peak at 916 eV decreases and a broad band at 885 eV disappears, revealing now the presence of Ce^{3+}. This can be also evidenced by following the diminishment of v'' peak and the appearance of the v' peak in Fig. 5b. This trend is in accordance with the gradual formation of a $CeVO_4$ phase. It is also corroborated by the evolution of V^{3+} population which is largely reported in the literature [30,32,42]. It could also be said that the formation of such phase appears to be in its very beginning in sample $Pt/6VCeO_2$ (peak at 513.9 eV), although it was not clearly detectable by the other techniques.

The binding energies of O1*s* are presented in Table 4 and the spectra are depicted in Fig. 5a. The peak centered at around 529.4 eV on Pt/CeO_2 is attributed to the oxygen in the oxide network of CeO_2 [45]. As for the other samples, the position of such peak gradually shifts towards higher binding energies as the amount of vanadium increases (Table 4); this feature may indeed be associated with the growing presence of Ce^{3+} as the O1*s* peak is positioned at 530.3 eV for the reduced Ce_2O_3 [45,46]. These findings are in line with the analysis of the Ce3*d* region discussed above. Nevertheless, some contribution from the presence of VO_x species may also be considered. In fact, the characteristic O1*s* binding energy value for V_2O_5 is 530.1 eV, which should contribute to the observed shift in the O1*s* spectra [47].

Another small peak can be found at higher binding energies (around 531.7 eV) for all samples and is attributable to ambient moisture [48], the presence of hydroxyl surface species, defects at the surface or oxygen ions with unusual coordination in a defective CeO_x ($x < 2$) [49].

The Pt4*f* region (not shown) was also studied and, for the majority of the samples, the collected spectra were fitted by two components. The main peak corresponded to the doublet $Pt4f_{7/2}/Pt4f_{5/2}$ that overlaps V3*s* region. According to the binding energies reported in the literature, the doublets can be ascribed to platinum in the metallic (Pt^0) and oxidized (Pt^{2+}) states [50]. In the spectra collected for the unmodified and $Pt/1VCeO_2$ samples, the Pt4*f* peak was well-defined and did not show the metallic spectral component. By increasing vanadium loading, the complete distinction of the different chemical states turned more difficult due to the complexity of the spectra, but an increase in the atomic percentage of Pt^0 was detected. The results clearly showed that the presence of vanadium directly influenced the distribution of platinum oxidation states. It is conceivable that the contact V–Pt could promote the reduction of Pt^{2+} ions to Pt^0 as it has a higher redox potential.

Table 4 presents the surface atomic composition, considering some atomic ratios. Even though a definitive procedure to estimate the total percentage of each cerium oxidation state in a sample has not been established yet and it is definitely an issue under open debate, the Ce^{4+}/Ce^{3+} values indeed suggest that the Ce^{3+} population increases along with vanadium content. The varying position of the peaks, their shape and width (Fig. 5b) lays no doubt on the existence of both Ce^{4+} and Ce^{3+} species or on their different distribution in each sample according to its chemical composition.

A drop in the Pt/(V + Ce) atomic ratio was observed for the highest vanadium loading samples (Table 4). This trend might suggest a lower platinum dispersion onto the supports as the bulk chemical analysis (Table 1) revealed that the samples present basically the same metal composition. Such effect on metal dispersion may have been brought about by the strong drop in surface area upon the preparation of vanadium-modified supports.

Finally, as expected, the calculated V/Ce ratio showed that the surface of the samples followed the same trend observed for the bulk composition (Table 1).

3.2. Drifts

The reduction of the catalysts by hydrogen was followed by DRIFTS as temperature increased. Figs. 6a–6b depicts the spectra for the unmodified Pt/CeO_2 and $Pt/6VCeO_2$ as representative of the vanadium-modified samples.

The spectra of the as-synthesized catalysts, taken at room temperature, show broad bands in the OCO vibration region (1800–1000 cm^{-1}) due to the massive presence of different adsorption modes of carbonates [51]. It is expected as CeO_2 is known by its capacity of adsorbing CO_2 and generating surface carbonate species even under storage conditions. The presence of all types of carbonates (monodentate, bidentate, polydentate and hydrogenocarbonate) may be considered as the spectra are quite complex and the distinction between the different species could always be questionable. Bands typically related to C–H vibrations within 2900–2800 cm^{-1} are also detected. By rising the temperature, these bands become weaker but the OCO vibration region definitely undergoes the most critical changes. Two bands at 1500 and 1375 cm^{-1} still remain even at temperatures as high as 350 °C, suggesting that the more thermally resistant carbonates, probably monodentate carbonates [53], are still present. The new absorptions arising at 200 °C (2037 and 1957 cm^{-1}) may result from

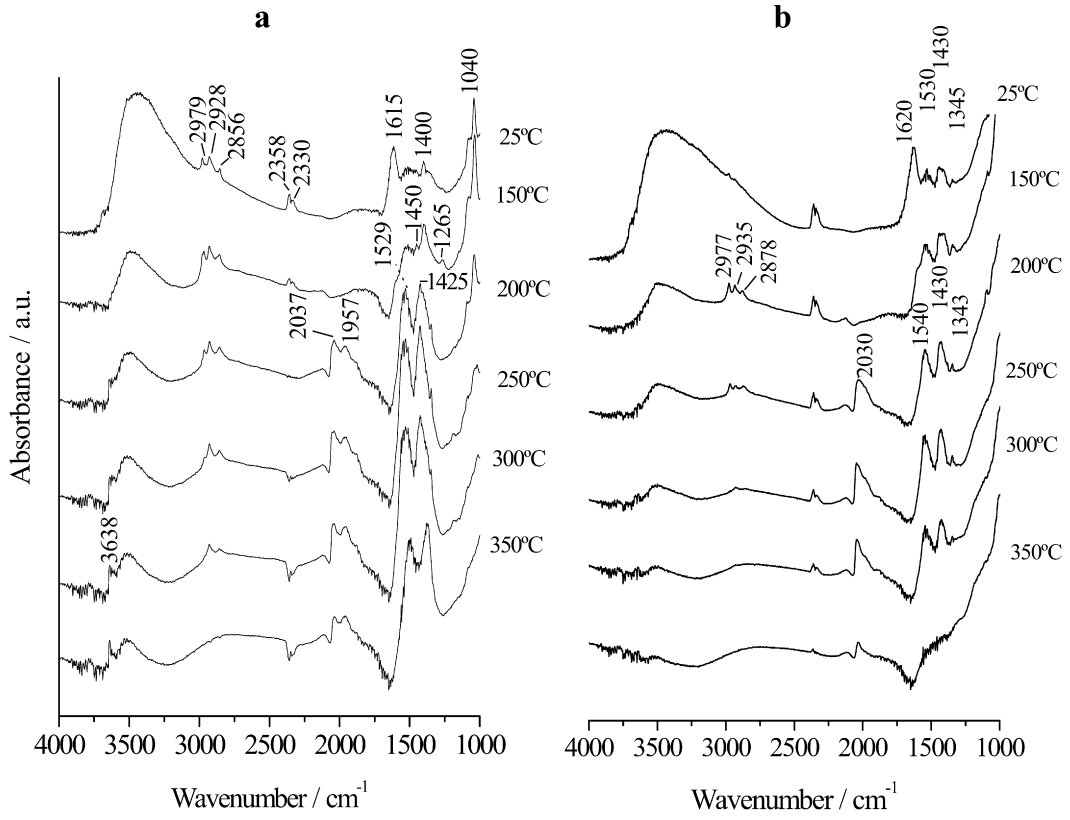

Fig. 6. DRIFTS spectra of the reduction step recorded under H_2 at the indicated temperatures over Pt/CeO_2 (a) and $Pt/6VCeO_2$ (b).

adsorption of CO, produced by decomposition of carbonates upon reduction, onto the just reduced Pt sites in the linear and bridged configurations, respectively.

A poorly-resolved band at 2115 cm^{-1}, which appears from 150 °C on, may be tentatively attributed to the vibration of a CO–Ce^{3+} bond or to an electronic transition of the reduced ceria as mentioned by Binet et al. [51]. Either case, this vibration is formed as a consequence of the reduction process of ceria surface promoted by the presence of metallic platinum sites.

Finally, it is also worth noting the hydroxyl vibration region between 3700–3200 cm^{-1}. The spectrum of the untreated support exhibits a broad band, typically observed over hydrated samples, which diminishes along with heating. The reduction process also leads to the generation of different OH groups, which are associated with the vibrations at 3638 and 3500 cm^{-1}, assigned to the Ce–OH vibrations and type II (bridged) and tridentate hydroxyl groups, respectively [52]. These frequencies become quite clearer as temperature increases, starting at 200 °C.

This reduction behavior is in close agreement with previous studies reported so far in the literature for similar catalytic systems [7,24].

The spectra of the vanadium-modified catalysts (Fig. 6b) revealed some differences upon reduction. Even though they are initially also characterized by the strong presence of different carbonate species, their thermal stability seems to be rather lower; as temperature raises, the OCO vibration features decrease and disappear completely at 350 °C, allowing a high level of superficial cleanness. This finding allows the conclusion that the formation and consequently the decomposition of carbonate species is deeply affected by the presence of vanadium.

Similarly to what was observed over the unmodified sample, CO formed by carbonate decomposition is adsorbed on both reduced Ce^{3+} (2115 cm^{-1}) and platinum (2030 cm^{-1}) sites. In this case, however, CO seems to be preferentially linearly adsorbed onto platinum metallic particles although a long tail towards lower wavenumbers can be observed.

In a second experiment, CO adsorption on the reduced catalysts was monitored. Firstly, the samples were reduced at 350 °C under hydrogen, purged in nitrogen and cooled down to 200 °C. A 3% CO/N_2 mixture was then admitted into the infrared cell at different temperatures: 200, 250 and 300 °C. The spectra for the unmodified and vanadium-modified Pt/CeO_2 catalysts are shown in Fig. 7. As can be seen, many adsorption bands emerge after CO adsorption irrespective of the temperature and catalyst composition. Moreover, the positions of the bands vary only slightly as the temperature raises and no significant differences between the spectra of the same sample are noted. However, the distribution of absorption bands in the OCO vibration region differs.

Pt/CeO_2 exhibited bands that could be attributed to different types of surface carbonates similarly to the discussion presented above about the reduction process. In this case, however, an additional band centered at 1725 cm^{-1} is observed and its intensity diminishes as the temperature increases.

It is worth mentioning that an assertive assignment of all bands in the spectra is rather difficult as the OCO stretching vibration region is pretty confusing since the absorptions may also be associated with formate species generated by the reaction of CO with the bridging OH groups formed upon reduction [7]. Indeed, C–H stretching vibrations are seen at 2970 and 2860 cm^{-1} in the spectra collected at the lower temperatures. As for the adsorption of CO at 300 °C, on the other hand, the bands related to such species cannot be detected. The remaining bands in the OCO region may thus be associated with the more thermally stable carbonates, especially the polydentate type. It should be observed that these bands are then less intense, suggesting that at lower temperatures both carbonate and formate species would contribute to the absorptions registered in the spectra of Pt/CeO_2.

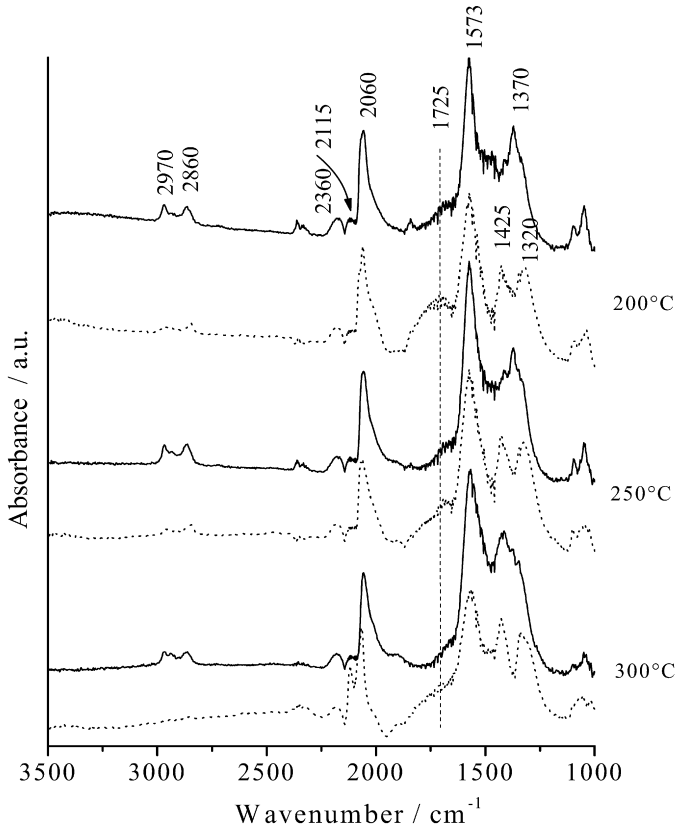

Fig. 7. DRIFTS spectra after CO adsorption; recorded under 3% CO at the indicated temperatures. solid line: $Pt/6VCeO_2$, dashed line: Pt/CeO_2.

In contrast, the $Pt/6VCeO_2$ catalyst exhibits basically two intense bands in the OCO region at 1573 and 1370 cm^{-1}; the vibration corresponding to polydentate carbonate is not observed. As the surface carbonate species emerge from the interaction between oxygen atoms with cerium cations, their chemical nature and geometry is straightly dependent on the exposed cerium centers onto the oxide surface. The dispersion of vanadia, and consequently the generation of VO_x species with V=O, V–O–V and especially V–O–Ce bonds, diminishes the available cerium surface cations. It is then conceivable that the formation of multicoordenated carbonates is inhibited on the vanadium-modified samples. These results therefore suggest that the OCO vibrations in the $Pt/6VCeO_2$ catalyst derive mainly from the formate created upon CO adsorption.

The band related to the adsorption of CO onto the metallic platinum particles (2060 cm^{-1}) are present in all spectra; it is observed that they are very similar for both catalysts revealing that CO is mostly linearly attached to metal particles.

3.3. Catalytic activity

As previously emphasized, all samples were tested considering an initial mixture of reactant gases prepared to simulate the composition reported by the partial oxidation of ethanol [26,27]. It must be kept in mind, however, that a significant amount of steam was added into the reformate stream before the mixture was admitted into the WGS reactor. The reaction rates calculated under differential conditions (CO conversions less than 15%) at 300 °C for the five ceria-based catalysts are listed in Table 5.

Comparing the performance of the Pt/CeO_2 sample with those reported so far in the literature is not straightforward as the activity is deeply influenced by the reaction conditions. After a broad examination of the literature, one can easily find that different groups have been using completely different operating conditions, being the gas composition one of the most dramatic issues. Even

Table 5
Reaction rates on WGS reaction at 300 °C

Catalysts	R (μmol g^{-1} s^{-1})
Pt/CeO_2	1.89
$Pt/1VCeO_2$	2.70
$Pt/6VCeO_2$	3.81
$Pt/12VCeO_2$	3.33
$Pt/18VCeO_2$	2.20

though the reaction rate has been shown to be independent of the CO partial pressure, the reaction order is around 0.5–1 with respect to water concentration, which implies in a significant effect of the H_2O/CO ratio used [53,54]. Moreover, many authors insist on disregarding the inhibiting effect of CO_2 and hydrogen, testing the catalyst with a simple CO/H_2O mixture. Therefore, any comparison among the extensive data available in the related literature must be done with extreme care as it has been wisely pointed out by some authors lately [53,55].

As concerning the addition of vanadia into Pt/CeO_2 catalyst formulation, it can be seen that regardless of the amount, it leads to an improvement in WGS activity. The apparent activation energy determined for Pt/CeO_2 and $Pt/6VCeO_2$, as representative of vanadia-modified catalysts (79 and 86 kJ/mol, respectively), are similar to those reported by some authors who have considered the effects of both CO_2 and H_2 in their kinetics studies [53,54,56]. These values were calculated within the same range of temperature and the well-fitted kinetic data are depicted in the Arrhenius plot presented in Fig. 8.

The positive effect in the WGS kinetics observed with the vanadia-promoted systems can be due to the molecular structure of the support surface since this is the more significant difference among them all as revealed by the spectroscopic studies reported herein. Therefore, a correlation between reaction rate and density

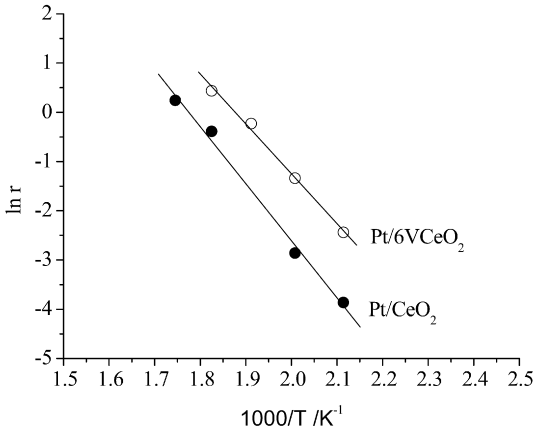

Fig. 8. Correlation between catalyst activity and surface vanadium density.

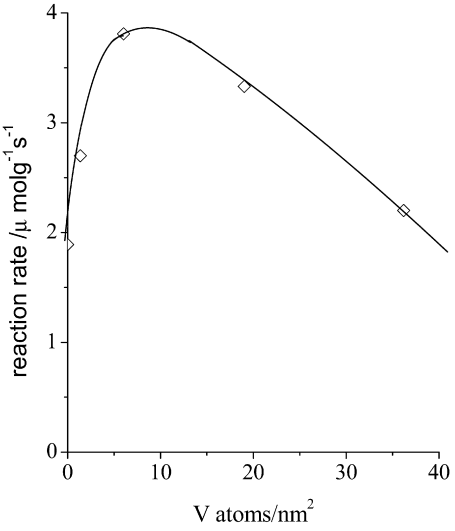

Fig. 9. Arrhenius plot for WGS reaction on Pt/CeO_2 and $Pt/6VCeO_2$ catalysts.

of VO_x species was tried and is depicted in Fig. 9. It was found that the rate increases up to a vanadium fraction corresponding to 6 V atoms/nm^2 and then continuously decreases for higher percentages. This experimental value is slightly below the monolayer coverage; therefore this finding suggests that once a monolayer is formed the promoting effect of vanadia species seems to be hindered.

As a matter of fact, considering the clear identification of crystalline tridimensional vanadium phases by XRD (Fig. 1) along with the appearance of Ce^{3+} due to the formation of $CeVO_4$ revealed by XPS (Fig. 5b), the results allow the conclusion that as soon as vanadia loading is high enough to generate such species the activity is negatively affected. Conversely, higher rates were accomplished at low-intermediate levels of 3 wt%. At this point, monovanadate is the predominant species with a lower proportion of polyvanadate as seen from UV–vis DRS.

Regarding the molecular structure of all species identified in the studied samples, monovanadate is a VO_4 entity with one V=O bond that points away from the surface of CeO_2 and three V–O–Ce bonds that link the V atom to the support. On the other hand, polyvanadate consists of VO_4 units bridged by V–O–V bonds so that each V atom gives rise to one V=O bond, two V–O–V bonds, and one V–O–Ce bond. Finally, tridimensional structures markedly feature V–O–V bonds with vanadyl groups terminally located. It may thus be suggested that the V–O–V bonds would play no role in the WGS reaction, otherwise $Pt/12VCeO_2$ and $Pt/18VCeO_2$ would

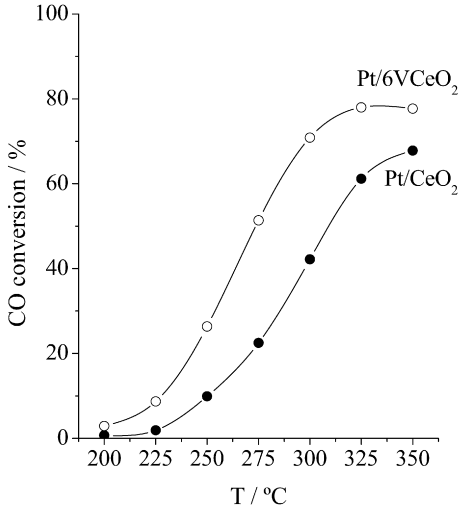

Fig. 10. CO conversion as a function of WGS reaction temperature over Pt/CeO_2 and $Pt/6VCeO_2$.

reach much higher rates as it was seen from all spectroscopic results that these samples are characterized by both polyvanadates and V_2O_5 moieties, species at which the V–O–V bonds are more numerous. Likewise, vanadyl groups could also be ruled out as they are present in all molecular configurations of VO_x species. In addition, their concentration readily increases as the vanadium loading increases, which should have led to a gradual improvement in the WGS kinetics. Consequently, the promoting effect of vanadium in these systems seems to be related to V–O–Ce bonds, which are available, accessible and at high concentration in the monovanadate species preferentially formed below the monolayer coverage.

At first, the improved kinetics of the WGS accomplished by adding vanadia can be rationalized if one considers that the reaction mechanism is a redox process. The deposition of vanadia on the surface of ceria results in a support with even enhanced reducibility, where labile oxygen to oxidize the adsorbed CO would be provided by ceria, monovanadate and, to a lesser extent, polyvanadate. The oxygen atoms in vanadium dispersed species is indeed very active as already recognized in other oxidation reactions [57,58].

Nonetheless, the DRIFTS results presented in this work do not allow ruling out the formate mechanism proposed in the literature. As seen from the infrared spectra (Figs. 6a–6b), formate species are generated on all samples, but by following the evolution of the related bands along with temperature a different trend in the decrease of the formate vibrations could be observed. Indeed, the decomposition of formate species was recorded at much lower temperature over vanadia-modified catalyst; a difference in temperature as high as 100 °C is found between the Pt/CeO_2 and the $Pt/6VCeO_2$. As the decomposition of these species is claimed to be the key step of the reaction, the disappearance of their vibrations in the infrared spectra would provide a measure of the catalyst activity. Indeed, the DRIFT spectra and the reaction rates are in pretty close agreement and evidence the benefits brought about by dispersing vanadium species onto the catalyst surface.

Finally, the CO conversion for the sample that exhibited the highest activity ($Pt/6VCeO_2$) was contrasted with unmodified Pt/CeO_2 over a wider range of temperatures (200 and 350 °C) as displayed in Fig. 10. The promoting effects of vanadia are remarkable over the whole temperature range investigated. It should also be mentioned that methanation reaction did not occur under any of the experimental conditions used.

4. Conclusion

Dispersion of vanadia onto Pt/CeO_2 increased the catalytic activity up to a vanadium surface density of 6 V atoms/nm^2, which is below the monolayer coverage. This concentration caused the formation of mono and polyvanadates species. Amongst all V–O bonds established in the molecular structure of vanadium species identified by different spectroscopic techniques, the improvement in WGS reaction kinetics is suggested to be associated with the V–O–Ce bonds. The generation of tridimensional structures with V–O–V bonds led to a gradual drop in activity.

Acknowledgments

The authors are indebted to Mr. Bruno Mello de Medeiros and Ms. Michelly Távora Rodrigues from INT for their experimental assistance. They thank Dr. Mona Abdel-Rehim (CETEM) for the chemical composition analyses. P.B. also acknowledges the grant provided by FAPESB. This work received financial support of CTENERG/FINEP-01.04.0525.00.

References

[1] C.H. Bartholomew, R.J. Farrauto, Fundamentals of Industrial Catalytic Processes, second ed., Wiley–Interscience, 2006, p. 909.
[2] X. Liu, W. Ruettinger, X. Xu, R. Farrauto, Appl. Catal. B 56 (2005) 69.
[3] W. Ruettinger, X. Liu, R. Farrauto, Appl. Catal. B 65 (2006) 135.
[4] T. Utaka, T. Okanishi, T. Takeguchi, R. Kikuchi, K. Eguchi, Appl. Catal. A 245 (2003) 343.
[5] C. Wheeler, A. Jhalani, E.J. Klein, S. Tummala, L.D. Schmidt, J. Catal. 223 (2004) 191.
[6] Q. Fu, A. Weber, M. Flytzani-Stephanopoulos, Catal. Lett. 77 (2001) 87.
[7] G. Jacobs, L. Williams, U. Graham, D. Sparks, B.H. Davis, J. Phys. Chem. B 107 (2003) 10398.
[8] G. Jacobs, P.M. Patterson, L. Williams, D. Sparks, B.H. Davis, Catal. Lett. 96 (2004) 97.
[9] G. Jacobs, S. Ricote, B.H. Davis, Appl. Catal. A 302 (2006) 14.
[10] T. Tabakova, F. Boccuzzi, M. Manzoli, J.W. Sobczak, V. Idakiev, D. Andreeva, Appl. Catal. A 298 (2006) 127.
[11] F.C. Meunier, D. Reid, A. Goguet, S. Shekhtman, C. Hardacre, R. Burch, W. Deng, M. Flytzani-Stephanopoulos, J. Catal. 247 (2007) 277.
[12] P.S. Querino, J.R.C. Bispo, M.C. Rangel, Catal. Today 107 (2005) 920.
[13] P. Panagiotopoulou, D.I. Kondarides, Catal. Today 112 (2006) 49.
[14] Q. Fu, W. Deng, H. Saltsburg, M. Flytzani-Stephanopoulos, Appl. Catal. B 56 (2005) 57.
[15] J.M. Pigos, C.J. Brooks, G. Jacobs, B.H. Davis, Appl. Catal. A 319 (2006) 47.
[16] H. Iida, A. Igarashi, Appl. Catal. A 298 (2006) 152.
[17] G. Jacobs, P.M. Patterson, U.M. Graham, A.C. Crawford, A. Dozier, B.H. Davis, J. Catal. 235 (2005) 79.
[18] E. Chenu, G. Jacobs, A.C. Crawford, R.A. Keogh, P.M. Patterson, D.E. Sparks, B.H. Davis, Appl. Catal. B 59 (2005) 45.
[19] A.M. Duarte de Farias, A.P.M.G. Barandas, R.F. Perez, M.A. Fraga, J. Power Sources 165 (2007) 854.
[20] S. Bernal, J. Kaspar, A. Trovarelli, Catal. Today 20 (1999) 173.
[21] S. Ricote, G. Jacobs, M. Milling, Y. Ji, P.M. Patterson, B.H. Davis, Appl. Catal. A 303 (2006) 35.
[22] N. Ballarini, A. Battist, F. Cavani, A. Cericola, C. Lucarelli, S. Racioppi, P. Arpentinier, Catal. Today 116 (2006) 313.
[23] A.M. Silva, A.M. Duarte de Farias, L.O.O. Costa, A.P.M.G. Barandas, L.V. Mattos, M.A. Fraga, F.B. Noronha, Appl. Catal. A 334 (2008) 179.
[24] J. Haber, M. Witko, R. Tokarz, Appl. Catal. A 157 (1997) 3.
[25] S. Letichevsky, C.A. Tellez, R.R. De Avillez, M.I.P. Silva, M.A. Fraga, L.G. Appel, Appl. Catal. B 58 (2005) 203.
[26] A.M. Silva, A.P.M.G. Barandas, L.O.O. Costa, L.E.P. Borges, L.V. Mattos, F.B. Noronha, Catal. Today 297 (2007) 129.
[27] A.M. Silva, L.O.O. Costa, A.P.M.G. Barandas, L.E.P. Borges, L.V. Mattos, F.B. Noronha, Catal. Today 755 (2008) 133.
[28] M.A. Bañares, M.V. Martínez-Huerta, X. Gao, J.L.G. Fierro, I.E. Wachs, Catal. Today 61 (2000) 295.
[29] W. Daniell, A. Ponchel, S. Kuba, F. Anderle, T. Weingand, D.H. Gregory, H. Knözinger, Top. Catal. 20 (2002) 65.
[30] M.V. Martínez-Huerta, J.M. Coronado, M. Fernández-García, A. Iglesias-Juez, G. Deo, J.L.G. Fierro, M.A. Bañares, J. Catal. 225 (2004) 240.
[31] T. Radhika, S. Sugunan, Catal. Commun. 8 (2007) 150.
[32] B.M. Reddy, B. Chowdhury, I. Ganesh, E.P. Reddy, T.C. Rojas, A. Fernández, J. Phys. Chem. B 102 (1998) 10176.
[33] A. Khodakov, J. Yang, S. Su, E. Iglesia, A.T. Bell, J. Catal. 177 (1998) 343.
[34] I. Georgiadou, C. Papadopoulou, H.K. Matralis, G.A. Voyiatzis, A. Lycourghiotis, C. Kordulis, J. Phys. Chem. B 102 (1998) 8459.
[35] X. Gao, I.E. Wachs, J. Phys. Chem. B 104 (2000) 1261.
[36] I.E. Wachs, J. Jehng, G. Deo, B.M. Weckhuysen, V.V. Guliants, J.B. Benziger, Catal. Today 32 (1996) 47.
[37] R. Zimmerman, R. Claessen, F. Reinet, P. Steiner, S. Huffner, J. Phys. Condens. Matter 10 (1998) 5697.
[38] G. Silversmit, D. Depla, H. Poelma, G.B. Marin, R. Gryse, J. Electron. Spectrosc. Relat. Phenom. 134 (2004) 167.
[39] Y. Suchorski, L. Rihko-Struckmann, F. Klose, Y. Ye, M. Alandjiyska, K. Sundmacher, H. Weiss, Appl. Surf. Sci. 249 (2005) 231.
[40] A. Pfau, K.D. Schierbaum, Surf. Sci. 321 (1994) 71.
[41] S. Damyanova, J.M.C. Bueno, Appl. Catal. A 253 (2003) 135.
[42] G.S. Wong, J.M. Vohs, Surf. Sci. 498 (2002) 266.
[43] T. Feng, J.M. Vohs, J. Catal. 221 (2004) 619.
[44] J.Z. Shyu, K. Otto, W.L.H. Watkins, G.W. Graham, R.K. Belitz, H.S. Gandhi, J. Catal. 114 (1988) 22.
[45] E. Abi-Aad, R. Bechara, J. Grimblot, A. Aboukaïs, Chem. Mater. 5 (1993) 793.
[46] S. Surnev, M.G. Ramsey, F.P. Netzer, Prog. Surf. Sci. 73 (2003) 117.
[47] J. Biener, M. Bäumer, R.J. Madix, P. Liu, E.J. Nelson, T. Kendelewicz, G.E. Brown, Surf. Sci. 441 (1999) 1.
[48] J. Matta, D. Courcot, E. Abi-Aad, A. Aboukaïs, J. Therm. Anal. Calorim. 66 (2001) 717.
[49] J.P. Holgado, G. Munuera, J.P. Espinós, A.R. González-Elipe, Appl. Surf. Sci. 158 (2000) 164.
[50] V.K. Kaushik, Phys. Chem. 173 (1991) 105.
[51] C. Binet, M. Daturi, J.C. Lavalley, Catal. Today 50 (1999) 207.
[52] A. Holmgren, B. Andersson, D. Duprez, Appl. Catal. B 22 (1999) 215.
[53] A.A. Phatak, N. Koryabkina, S. Rai, J.L. Ratts, W. Ruettinger, R.J. Farrauto, G.E. Blau, W.N. Delgass, F.H. Ribeiro, Catal. Today 123 (2007) 224.
[54] G. Germani, P. Alphonse, M. Courty, Y. Schuurman, Catal. Today 110 (2005) 114.
[55] O. Thinon, F. Diehl, P. Avenier, Y. Schuurman, Catal. Today 137 (2008) 29.
[56] R. Radhakrishnan, R.R. Willligan, Z. Dardas, T.H. Vanderspurt, Appl. Catal. B 66 (2006) 23.
[57] H. Tian, E.I. Ross, I.E. Wachs, J. Phys. Chem. B 110 (2006) 9593.
[58] B.M. Weckhuysen, D.E. Keller, Catal. Today 78 (2003) 25.